

# Application of USAXS analysis and non-interacting approximation to determine the influence of process parameters and ageing on the thermal conductivity of electron-beam physical vapor deposited thermal barrier coatings

A. Flores Renteria<sup>a,\*</sup>, B. Saruhan<sup>a</sup>, J. Ilavsky<sup>b</sup>, A.J. Allen<sup>c</sup>

<sup>a</sup> German Aerospace Center (DLR), Institute of Materials Research, Linder Hoehe, 51147, Cologne, Germany

<sup>b</sup> Argonne National Laboratory, Advanced Photon Source (APS), 9700 S. Cass Avenue, bldg 438E Argonne, IL 60439, USA

<sup>c</sup> National Institute of Standards and Technology (NIST), 100 Bureau Drive, Gaithersburg, MD 20899, USA

Received 9 August 2006; accepted in revised form 11 October 2006

Available online 21 November 2006

## Abstract

Electron-beam physical vapor deposited (EB-PVD) thermal barrier coatings (TBCs) display a lower thermal conductivity compared with the deposited bulk material. This effect is achieved due to the presence of pores within these films. The spatial and geometrical characteristics of the porosity influence directly the magnitude of the achieved reduction of the thermal conductivity. In this work, three EB-PVD coating containing different microstructures were manufactured by varying the manufacturing process parameters during the deposition process. Their corresponding thermal conductivities were measured via the laser flash analysis method (LFA) in both the as-coated state and after ageing (1100 °C/100 h). Analysis of the pore formation during processing was carried out by ultrasmall-angle X-ray scattering (USAXS). This technique is supported with a computer based modeling developed by researchers at Advanced Photon Source (APS) in ANL, USA, and in National Institute of Standards and Technology (NIST), USA. The model enables the characterization of the size, shape, volume and orientation of each of the pore populations in EB-PVD TBCs. The effect of these spatial and geometrical characteristics of the porosity on the thermal conductivity of the EB-PVD coatings were studied via a non-interacting approximation based on Maxwell's model. Results of LFA measurements and the applied approximation indicate an interrelation between the microstructure and the thermal properties of the analyzed EB-PVD coatings. Microstructures containing a higher volume fraction of fine anisotropic intra-columnar pores, and larger voids between feather-arms oriented at lower angles toward the substrate plane correspond to lower thermal conductivity values. Inter-columnar gaps do not significantly contribute to lowering the thermal conductivity due to their orientation parallel to the heat flux and their lower volume fraction compared with the volume occupied by the primary columns. On heat treatment, the deepest section of the gaps between feather-arms break-up into arrays of nano-sized low aspect ratio voids. The anisotropic, elongated intra-columnar pores evolve toward low aspect ratio shapes that are less effective in reducing the thermal conductivity. © 2006 Elsevier B.V. All rights reserved.

**Keywords:** Electron-beam physical vapor deposition; Thermal barrier coatings; Ultrasmall-angle X-ray scattering; Thermal conductivity modeling

## 1. Introduction

Thermal barrier coatings (TBCs) produced via electron-beam physical vapor deposition (EB-PVD) are employed to protect the metallic blades of aircraft turbines exposed to high-temperature cyclic conditions during in-service lifetime. Such coatings are specifically suitable for this purpose because of their appropriate

thermo-mechanical properties, protecting components exposed to high temperature thermo-cyclic conditions [1–3]. EB-PVD process parameters such as substrate temperature and rotation speed influence strongly the morphological development of these coatings. As described by Schulz et al. [4], there is a direct relation between the rotation of substrates during coating and the growth and population of the primary columns in a preferred crystallographic direction (i.e. perpendicular to the substrate plane) as well as the formation of inter-columnar gaps between these columns. At the same time, development of intra-columnar

\* Corresponding author. Tel.: +49 2203 6012560; fax: +49 2203 696480.

E-mail address: [arturo.flores@dlr.de](mailto:arturo.flores@dlr.de) (A.F. Renteria).

pores occurs in an oblique orientation within the columns during every rotation movement (“sunrise–sunset” cycle). In addition, formation of secondary columns (so-called feather-arms) and gaps between them occurs near the periphery of each primary column, containing the same crystallographic orientation as the intra-columnar pores (see Fig. 4).

The presence of this complex porosity system in partially-yttria-stabilized zirconia (PYSZ) EB-PVD TBCs is assumed to be responsible for the reduction of the thermal conductivity compared with the intrinsic value for PYSZ bulk material (approx. 2 W/mK) [5,6], since thermal conductivity reflects a structural rather than an intrinsic physical property [7]. Thus, given the parallel arrangement of primary columns and inter-columnar gaps within the coatings, each of these features spans the same thermal gradient and most of the heat flow will occur through the coating via the better conductor, i.e., the columns [8]. Moreover, the nano-sized pores within the primary columns will interrupt the heat flow because of their inefficient conduction capacity, even when they are gas filled [9]. The effectiveness of the pores in impeding the heat flow must then depend on the effective surface area of each pore subtended to the plane perpendicular to the heat flux and their spatial distribution. As a result, control of the pore volume fraction, spatial distribution, orientation and morphology provides an approach for obtaining thermal barrier coatings with optimized thermal conductivity [10].

## 2. Theory

### 2.1. Ultrasmall-angle X-rays scattering analysis (USAXS)

When an X-ray beam passes through a porous sample, some of the X-rays are scattered out of the incident beam direction by a small angle. The intensity profile in scattering angle of this small-angle scattered component is effectively a Fourier transform of the solid/pore microstructure. A USAXS instrument, such as that at APS sector 33-ID, employs a Bonse–Hart optics design that enables the scattering to be accurately measured over a particularly large range of scattering angles with high resolution. From USAXS data, the pore morphology in a feature scale range from a few nanometers up to more than a micrometer can be characterized and quantified [11]. Analysis by USAXS has been successfully employed to characterize, separately, the stereometric (geometrical and spatial) information for each pore population that comprises the anisotropic porosity within EB-PVD TBCs [11,12]. The USAXS information obtained was used to model the overall thermal conductivity of these materials by using a non-interacting pore approximation constrained by the measured total pore volume. For the thermal conductivity analysis of a material containing anisotropic or non-spherical pores it is not sufficient to consider only the volume fraction of the consolidating phases (using the rule of mixtures); the spatial and geometrical characteristics of the non-continuous phase (i.e. pores) must also be taken in to account. Thus, the analysis of the influence of each pore population on the thermal conductivity of EB-PVD TBCs will be explored using this approach and validated by the experimental values.

In some cases the USAXS modeling considers stereometric values for two real pore populations to represent the fine and coarse sections of a single group of pores (e.g. inter-columnar gaps, gaps between feather arms, intra-columnar pores) in the EB-PVD TBCs model (see Fig. 3). Moreover, since USAXS analysis of the microstructures were experimentally carried out in two orthogonal directions (i.e. perpendicular and parallel to the axis of substrate rotation), there is also a group of modeled pore populations that share the stereometric characteristics of a single pore group (i.e. inter-columnar gaps, voids between feather-arms, or intra-columnar pores) within the real microstructure. Under these circumstances, the rule of mixtures was applied to obtain representative values of the factors used in the thermal conductivity calculations:

$$k_r = \sum_{i=1}^n k_i \left( \frac{V_i}{\sum_{i=1}^n V_i} \right) \quad (1)$$

where  $k_r$  is the representative thermal conductivity value of one pore-group domain,  $k_i$  and  $V_i$  are the thermal conductivity and volume fraction of one single USAXS pore population.

### 2.2. Thermal conductivity modeling

To analyze the influence of the pores on the thermal conductivity of EB-PVD TBCs, it is necessary to model the experimental values. This work applies the semi-empirical approximation of Lu [9] to calculate the thermal conductivity of three microstructures both as-coated and aged (1100 °C/100 h). In order to make the right approximations, it is necessary to use the stereometric data obtained by USAXS measurements. These approximations are based on Maxwell’s non-interaction scheme [13], assuming that the pores are thermal isolators and that the stereometric characteristics, as well as their volume fraction, control the thermal conductivity of a porous material.

According to the Lu model, the thermal conductivity tensor  $\bar{k}$  of a material containing pores of given shape and volume fraction,  $\Phi$  is given by

$$\frac{\bar{k}}{k_s} = 1 - \sum_i H_i(k_p/k_s, \Phi, \text{pore morphology}) \quad (2)$$

where  $H_i$  is the influence tensor of the  $i$ th pore group,  $k_p$  the effective pore conductivity and  $k_s$  the solid bulk material conductivity. Since the pores groups within EB-PVD TBCs are distributed in shape and spatial arrangement across the coating’s in-plane direction, the “pore morphology” is replaced by probability densities (detailed description in Refs. [9,14]). It is known that principally the size of the inter-columnar gaps and voids between feather-arms changes along the out-of-plane direction; this effect is not considered in this model, but a representative averaged value (USAXS pore population) obtained from USAXS analysis is used. Specific to the EB-PVD

TBC columnar microstructure (see Fig. 2) the overall thermal conductivity of the coating ( $k_{\text{coat}}$ ) is related to that of the columns by

$$\frac{k_{\text{coat}}}{k_{\text{col}}} = (1 - \Phi_{\text{iep}}) \sin^2 \omega \quad (3)$$

where  $k_{\text{col}}$  and  $\Phi_{\text{iep}}$  are the thermal conductivity of the individual columns and the volume fraction of the inter-columnar gaps, respectively, and  $\omega$  is the angle formed by the pores axis and the substrate's plane. Moreover, for the gaps between feather-arms, two morphologies can be considered in the model: oblate and prolate. For the confined thermal conductivity at this domain where the gaps between feather arms interact with the PYSZ bulk solid material ( $k_{\text{fag}}$ ), it is considered that these features are embedded within a domain containing intra-columnar pores having thermal conductivity,  $k_{\text{iap}}$ .

For oblate shapes:

$$\frac{k_{\text{fag}}}{k_{\text{iap}}} = (1 - \Phi_{\text{fag}}) \sin^2 \omega + \left( 1 - \frac{8}{3} \left[ \left( \frac{3}{4\pi} \right) \left( \frac{d}{t} \right) \Phi_{\text{fag}} \right] \right) \cos^2 \omega \quad (4)$$

For prolate shapes:

$$\frac{k_{\text{fag}}}{k_{\text{iap}}} = (1 - \Phi_{\text{fag}}) \sin^2 \omega + (1 - 2\Phi_{\text{fag}}) \cos^2 \omega \quad (5)$$

where  $d$  and  $t$  are the diameter and thickness of the ellipsoidal pores, respectively; and  $\omega$  is the angle between the axial dimension of the pores and the substrate's plane. The conductivity of the domain containing only intra-columnar pores interacting with the PYSZ bulk material is calculated by the same Eqs. (5) and (6) by changing the denominator  $k_{\text{iap}}$  to  $k_{\text{s}}$ , respectively. Additionally, for the case of spherical pores

$$\frac{k_{\text{iap}}}{k_{\text{s}}} = 1 - \frac{3\Phi_{\text{iap}}}{2} \quad (6)$$

Finally the value of the thermal conductivity in the columns forming the coatings is related to the gaps between feather arms domain ( $k_{\text{fag}}$ ) and intra-columnar pores domain ( $k_{\text{iap}}$ ) by their corresponding cross-section area fraction perpendicular to the heat flux in each primary column ( $S_{\text{fag}}$  and  $S_{\text{iap}}$ , respectively)

$$k_{\text{col}} = (k_{\text{fa}} \cdot S_{\text{fa}}) + (k_{\text{ia}} \cdot S_{\text{ia}}) \quad (7)$$

Thus, the stereometric characterization of the porosity is presented for each of the three distinctive EB-PVD microstructures, via the USAXS analysis. Moreover, the obtained data is used as input for a non-interacting approximation derived from the Maxwell scheme that then predicts the overall thermal conductivity of the coatings.

### 3. Experimental

#### 3.1. Materials and fabrication methods

The PYSZ coatings were manufactured via the EB-PVD process by employing “von Ardenne<sup>1</sup>” pilot plant equipment having a maximum EB Power of 150 kW. Evaporation was carried out from a single evaporation source having an ingot form of 62.5 mm diameter and 150 mm length. The chemical composition of the ingot was 7–8 wt.% mass  $\text{Y}_2\text{O}_3$  stabilized  $\text{ZrO}_2$ . During the coating process at constant chamber pressure (0.8 Pa), the substrate rotation speed and temperature were varied in order to produce three different morphologies: “coarse” (3 rpm/1000 °C), “intermediate” (12 rpm/950 °C), and “feathery” (30 rpm/850 °C). A plane deposition of the vapor phase on the substrates was carried out using a conventional rotating mode (as described in Ref. [4]) by mounting the substrate on a holder with its rotation axis perpendicular to the evaporation source. EB-PVD PYSZ coatings of approx. 400  $\mu\text{m}$  thickness were deposited on Ni-base substrates previously coated with a NiCoCrAlY bond coat. USAXS specimens were prepared by cutting and polishing 200  $\mu\text{m}$  thick slices from the deposited coatings. Two orthogonal slices per specimen (perpendicular and parallel to the axis of substrate rotation) were prepared. For the thermal conductivity measurements via laser flash analysis method (LFA), the coatings were also deposited on FeCrAl-alloy substrates (without bond coat) in the form of 12.7 mm diameter discs during the same runs. Subsequently, the FeCrAl-alloy substrates were chemically etched away to obtain free-standing coating samples. These were additionally coated on both sides with a thin Pt layer via sputtering in order to avoid laser penetration during the measurements. Finally, corresponding USAXS and LFA specimens were heat treated in air at 1100 °C/100 h using a heating rate of 5 °C/min.

#### 3.2. Characterization methods

Statistically representative and quantitative stereometric characterization of the anisotropic pores in the analyzed EB-PVD microstructures was achieved by employing an effective-pinhole collimated USAXS instrument and its supporting data processing system. The measurements were carried out using the USAXS instrument at UNICAT sector 33-ID at the Advance Photon Source Synchrotron, Argonne National Laboratory, USA (detailed description in Ref. [15]). The raw data were corrected for background scattering, sample attenuation and multiple scattering. Then, computer modeling was used to obtain values of stereometric (geometrical and spatial) characteristics of the pore populations in terms of their volume fraction, shape (aspect ratio), size and orientation; each representing statistical average values based on Gaussian distributions [16]. The USAXS model utilizes five pore populations for the fitting process. The values obtained were correlated with Scanning Electron Microscope micrographs (FE-SEM, LEITZ LEO 982<sup>1</sup>) of the polished sections. Since the

<sup>1</sup> Information on commercial products is given for completeness and does not constitute or imply their endorsement by the National Institute of Standards and Technology.

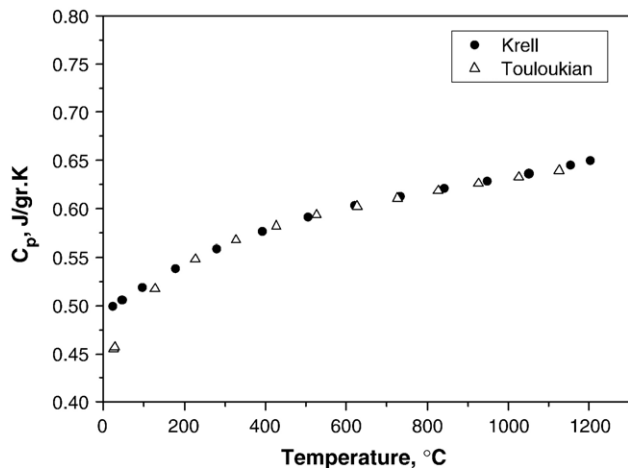


Fig. 1. Specific heat ( $C_p$ ) values of a 8 wt.% mass  $Y_2O_3$  stabilized  $ZrO_2$  heat treated powder according to the measurements reported by Krell [17] and Touloukian and Buyco [1].

different pore groups in EB-PVD TBCs contain highly anisotropic characteristics with only a limited degree of symmetry, for the application of the USAXS modeling each specimen was measured in at least two orthogonal directions: perpendicular and parallel to the axis of substrate rotation.

### 3.3. Thermal conductivity measurements

The thermal diffusivity ( $\alpha$ ) of the Pt-coated free-standing specimens was measured employing a Netsch-LFA 427<sup>1</sup> instrument. The corresponding thermal conductivity was calculated through the formula  $\lambda = \alpha \cdot \rho \cdot C_p$ , where  $\lambda$  is the thermal conductivity,  $\rho$  represents in this case the bulk density of the free-standing coatings measured by the Archimedes Method and  $C_p$  is the specific heat measured by differential scanning calorimeter (DSC) reported by Krell [17]. This data was obtained using a PYSZ powder, which was previously heat treated in order to liberate internal stresses. Fig. 1 shows the resulting  $C_p$  values and those obtained by using the rule of mixtures with the

data reported by Touloukian and Buyco [18] for an 8 wt.% mass  $Y_2O_3$ - $ZrO_2$  chemical composition.

## 4. Results and discussion

The three analyzed coatings display the typical columnar structure of EB-PVD PYSZ coatings, but with evident differences in the column diameter, as in the configuration of the gaps between the feather-arms and intra-columnar pores (see Figs. 2 and 4). The “coarse” microstructure contains larger column diameters and the “feathery” microstructure more pronounced feather-arm features (Fig. 2). The numerical data obtained by USAXS analysis and SEM micrograph observation indicate that basically all the investigated microstructures show variations in the pore distribution and differences in the cross-sectional column density of both, the perpendicular and parallel directions to the axis of substrate rotation. In the as-coated state, the inter-columnar gaps are slightly wider, and contain evidently higher volumes for the direction perpendicular to the axis of substrate rotation compared with the parallel direction for all the three analyzed coatings. Previous studies delivered similar qualitative results solely relying on microstructural investigations [19]. For all three analyzed microstructures (slices), the USAXS modeling identified individual pore groups that can be listed in two populations within a morphological category (e.g. intra-columnar voids “coarse” and “fine”) due to differences in their cross-section. Moreover, the USAXS modeling for the measured gaps between the feather-arms (i.e. secondary columns) yields also two populations: one of these groups concerns the widest part of these features which form the periphery of the column surface (coarse); the second group concerns the thinnest section of these features, localized deep within the column core (fine) (see Figs. 3 and 4a–c). Furthermore, intra-columnar pores were considered to be composed of two sections: (a) a nucleation oblate section, created at regions of highest vapor incident angles (VIA) where the edge of the deposited vapor after each complete rotation overlap with the initial growth generated by the next rotation’s movement; and (b) a growing prolate section, which is created by the growth of the formed pores through the deposited material parallel to the plane of the feather-arms in an

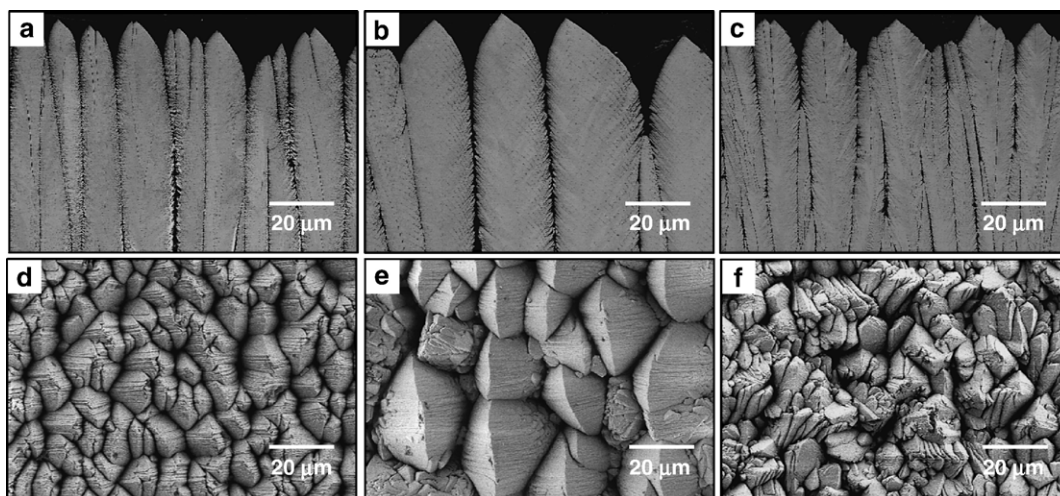


Fig. 2. Columnar structure of the three analyzed EB-PVD TBCs: (a) “Intermediate”, (b) “Coarse”, and (c) “Feathery”.

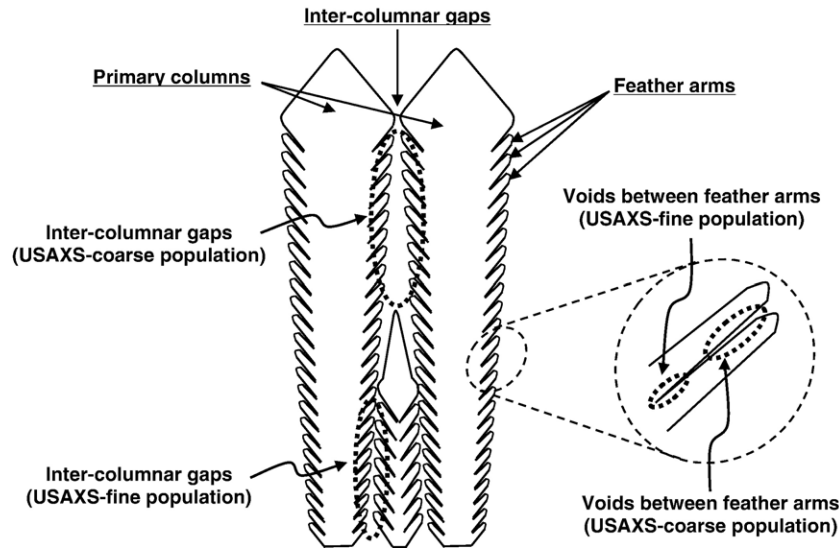


Fig. 3. Scheme of the USAXS populations representing the wide distribution of inter-columnar gaps and voids between feather arms in EB-PVD coatings.

elongated “banana” shape resulting from the changing direction of the VIA in a “sunrise–sunset” pattern (see Fig. 4d–f). Furthermore, it was observed that there were divergences in the values of the overall volume fraction of the porosity between the USAXS modeling data and the Archimedes Method. The USAXS modeling estimates higher volume fractions for the pores measured in the direction perpendicular to the axis of substrate rotation, and lower volume fractions for the pores determined in the orthogonal parallel direction. This effect results due to the highly anisotropic distribution of the porosity in these coatings. An oblique incidence of the vapor on the growing surfaces occurs primarily shadowed by ridges oriented parallel to the axis of substrate rotation. These edges are the principal features controlling the shadowing effect responsible for the anisotropic growth of the columns and the corresponding porosity formation. This configuration originates an elongation of the columns shape

in a direction parallel to the axis of substrate rotation, which encloses a corresponding anisotropic distribution of the porosity (see Fig. 2d–f). This phenomenon produces the formation of mainly wide inter-columnar pores oriented around the plane perpendicular to the plane of vapor incidence (PVI), and a higher volume fraction of the corresponding gaps between feather-arms at their periphery, and intra-columnar pores within the columns. The resulting volume fractions of each pore population calculated with the USAXS model were scaled to the corresponding total porosity volume measured with the Archimedes Method for each microstructure, ( $27.46 \pm 0.64\%$  for “feathery”,  $27.15 \pm 0.78\%$  for “intermediate”, and  $22.55 \pm 1.10\%$  for “coarse”). Since the resulting pore volume changes after ageing are slower than the uncertainties of the measuring technique, these values are considered to remain constant in the coated and heat treated conditions. The Fig. 5a shows the scaled volume fractions of the

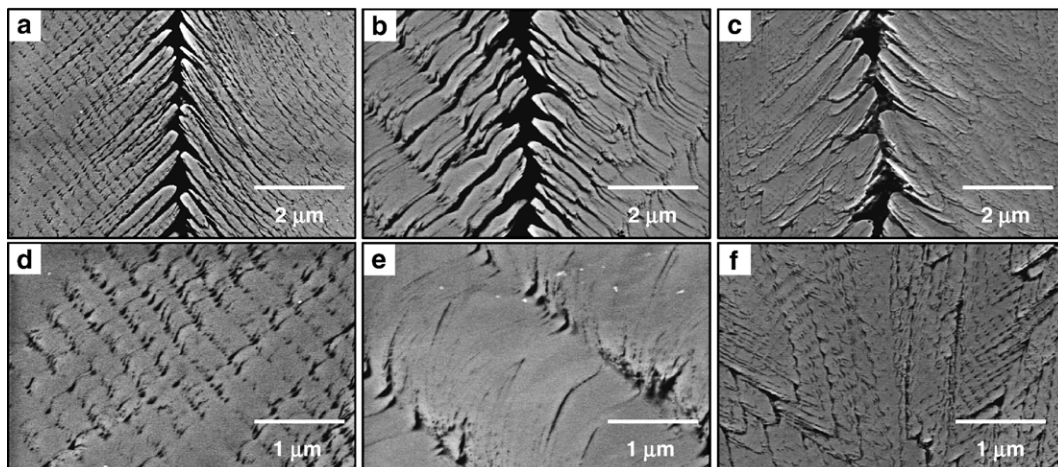


Fig. 4. SEM micrographs showing the configuration of the porosity within the cross-section of the primary columns in the direction perpendicular to the axis of substrate rotation of the three analyzed EB-PVD TBCs in as-coated conditions. The porosity is composed of gaps between feather arms: (a) “Intermediate”, (b) “Coarse”, and (c) “Feathery”; and intra-columnar pores: (d) “Intermediate”, (e) “Coarse”, and (f) “Feathery”.

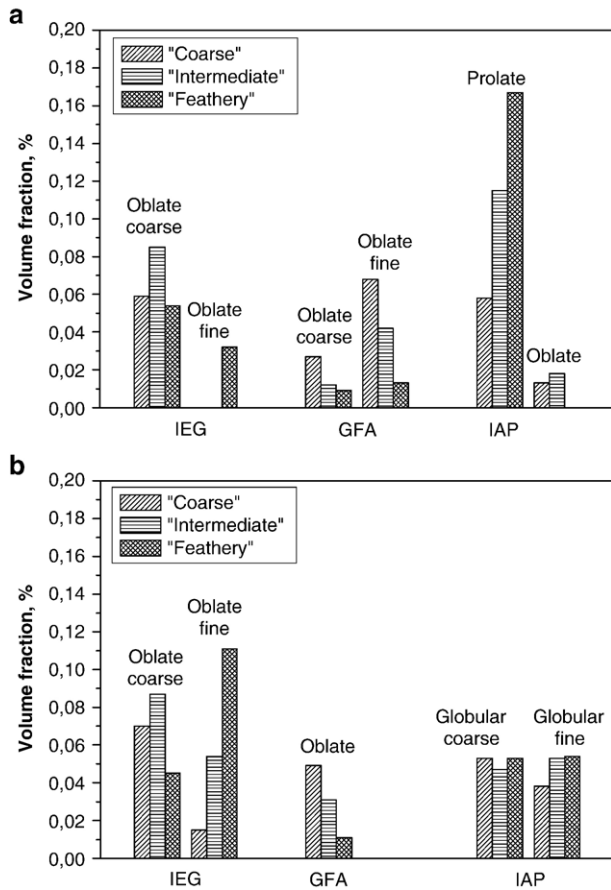


Fig. 5. Distribution of the averaged USAXS-modeled volume fractions of the different pores measured in the cross-section perpendicular to the axis of substrate rotation (inter-columnar gaps (IEG), gaps between feather arms (GFA), and intra-columnar pores (IAP)) within the analyzed EB-PVD TBCs (“Coarse”, “Intermediate”, and “Feathery”) in as-coated (a) and aged (1100 °C/100 h) conditions (b).

different pore groups and populations determined in the cross-section oriented perpendicular to the axis of substrate rotation of the analyzed EB-PVD microstructures. Looking at our resulting

data and considering errors during the measurements we believe that the stereometric values obtained via the USAXS-model contain uncertainties of approx. 10%.

The sintering process becomes active during heat treatment at 1100 °C for 100 h. Change of all pores after the ageing process into lower aspect-ratio shapes was evident in the different USAXS-modeled aspect ratio values and the micrographs in Fig. 6. This phenomenon clearly indicates the effect of sintering, which controls the shape of the pores enhanced by their surface area reduction. Previous investigations demonstrate that the surface area changes of the porosity in EB-PVD PYSZ TBCs during ageing at high temperatures ( $\geq 900$  °C) occurs by surface diffusion [20]. Then, the volume fraction of the evolved features should remain unaltered by the activation of sintering. However, the discrepancies between the volume fractions before and after ageing (Fig. 5a and b) are influenced by parallel competitive phenomena occurring at the pore-solid material configurations.

In the inter-columnar gaps, the alteration of the initial distribution of the averaged volume fraction is enhanced by two factors: (a) mass transfer occurs between primary columns through bridging at the previously formed contact points between primary columns. Finer columns, concentrated mainly at the bottom (foot) zone of the coating and which are initially prevented from growing all through the coating thickness, tend to pull together and create finer channels between them: (b) The smoothness effect of the feather-arms tips enhances the opening dimensioning of the inter-columnar gaps.

At the same time, significant changes occur at the gaps between feather-arms. The fine section of the gaps between feather-arms located deep into the primary columns core disappears completely after breaking-up into arrays of globular intra-columnar pores. The exterior coarse section located at the edge of the feather-arms evolves into lower aspect ratio openings (see Figs. 5b and 6a–c).

Moreover, the prolate high aspect-ratio intra-columnar pores (fine “banana” shaped pores), connecting the two rows of pores created by each rotation phase, change into

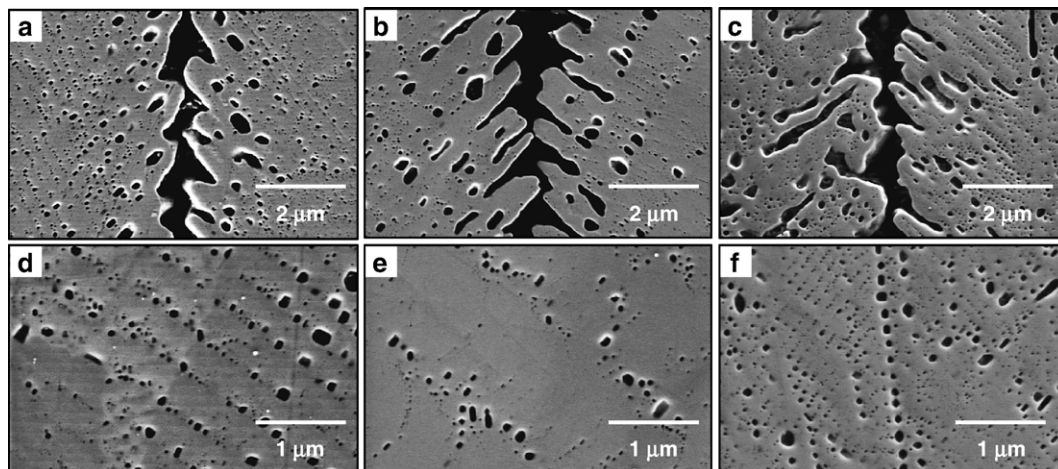


Fig. 6. SEM micrographs showing the configuration of the porosity within the cross-section of the primary columns in the direction perpendicular to the axis of substrate rotation of the three analyzed EB-PVD TBCs in aged conditions (1100 °C/100 h). The porosity is composed of gaps between feather arms: (a) “Intermediate”, (b) “Coarse”, and (c) “Feathery”; and intra-columnar pores: (d) “Intermediate”, (e) “Coarse”, and (f) “Feathery”.

Table 1

Modeled representative thermal conductivities of the pores-group domains within the analyzed EB-PVD microstructures in as-coated (AC) and heat treated (HT, 1100 °C/100 h) conditions: gaps between feather arms ( $k_{\text{fag}}$ ), and intra-columnar pores ( $k_{\text{iap}}$ ); and their corresponding modeled and measured thermal conductivity values ( $\lambda$ )

EB-PVD microstructure	Condition	Measured at 200 °C $\lambda$ , W/mK <sup>-1</sup>	Modeling $\lambda$ , W/mK	$k_{\text{coat}}/k_{\text{col}}$	$k_{\text{col}}$	$k_{\text{fag}}$	$k_{\text{iap}}$
Coarse	AC	1.65±0.10	1.67	0.924	1.816	1.516	1.898
	HT	1.76±0.12	1.77	0.943	1.882	1.714	1.899
Intermediate	AC	1.24±0.06	1.47	0.924	1.597	1.425	1.697
	HT	1.56±0.07	1.70	0.920	1.853	1.747	1.865
Feathery	AC	1.11±0.04	1.19	0.950	1.254	1.187	1.291
	HT	1.46±0.05	1.65	0.911	1.819	1.697	1.854

polydispersed globular pores (see Fig. 6d–f). The oblate section of these features evolves into a lower aspect ratio globular shape during ageing. A possible cause of the discrepancies in the volume fractions, especially in “intermediate” and “feathery” microstructures, could be a broader polydispersion of the pores size, since the USAXS modeling is limited to five pore populations. Even though the USAXS modeling considers a size distribution of 40% width, the characterization of intermediate sized pores in a broadly-polydispersed-size system is restricted. It is assumed that this effect originates the differences between the measured and calculated thermal conductivity of the “intermediate” and “feathery” microstructures.

The values of the modeled thermal conductivities corresponding to the analyzed EB-PVD TBCs reasonably agree with the measured experimental values and the interrelation between the different microstructures and their conditions (see Table 1). According to the thermal conductivities of the different pore-group domains given in Table 1, it is likely that the inter-columnar gaps will barely contribute to reducing the thermal conductivity due to their orientation being parallel to the heat flux ( $k_{\text{coat}}/k_{\text{col}}$ ). Furthermore, the low values of the thermal conductivity factor ( $k_{\text{fag}}$ ) at the gaps between feather-arms domain are primarily determined by the stereometric characteristics of the deepest fine section of the feather arms. These gaps interrupt the phonon flux by inserting oblique discontinuities (slices) within the columns, reaching a depth in each microstructure determined by the substrate temperature and rotation speed. These factors determine the mass diffusion effect and the shadowing “sunrise–sunset” effect of the neighboring column tips, respectively. Finally, the prolate sections of the intra-columnar pores ( $k_{\text{iap}}$ ) represent the principal factor governing the thermal conductivity reduction of the columns ( $k_{\text{col}}$ ) due to their larger volume fraction, size, and distribution within the cross-section area. This hypothesis is supported by the relationship between the volume fraction of the pores as defined by USAXS modeling (Fig. 5a), and their distribution in the cross-section of the primary columns (see Fig. 4d–f). This effect is confirmed by the agreement between the modeled and experimental thermal conductivity values and their interrelation for the three microstructures in the as-coated state (see Table 1).

The presence of a high amount of fine individual intra-columnar pores in the “feathery” microstructure is induced by the high rotation speed employed during the coating process, which causes the formation of large populations of new pore

arrays during the growth of the columns. Moreover, the lower substrate temperature, which is specific to the coating process of this microstructure, impedes the diffusion of atoms between the growing multiple “banana” shaped fronts and enhances the subsistence of these pores all through the material deposited in one single rotation phase until the next contact of the growing surface with the incident of vapor plane occurs. This process repeats until the intra-columnar pores, which are initially created in the middle of the columns, reach the column periphery forming feather-arms. Under thermal flux conditions, it is very likely that the phonons flowing through the columns will be stopped or scattered by this pore configuration.

In the case of the “intermediate” and “coarse” microstructures, larger intra-columnar pores are both anticipated and measured due to the lower rotation speeds during processing. Moreover, since these coatings are manufactured at higher substrate temperatures, only a smaller fraction of the pores are able to continuously grow at each rotation phase and survive until the next array of new pores is created. These coatings contain a smaller volume fraction of less uniformly distributed intra-columnar pores, thus resulting in higher thermal conductivity values (Fig. 5a and Table 1).

After heat treatment (1100 °C/100 h), the anisotropic and high-aspect ratio intra-columnar pores and the deepest-section of the gaps between the feather arms change into globular pores. This change produces a decrease in the cross-section surface area contributed by the formed low-aspect ratio intra-columnar pores, which together with their volume fraction, principally determines the final thermal conductivity values of the coatings (see Table 1 and Fig. 5b).

Nevertheless, the resulting pore configuration in the “feathery” microstructure is still more effective in reducing the thermal conductivity than in the “intermediate” and “coarse” microstructures. This can be mainly attributed to pore-size polydispersity and distribution within the cross-section area of the columns (see Fig. 6a–f). Consequently, a different equilibrium configuration of pores results from the sintering process, altering the effectiveness of the pores in interrupting the heat transfer through the coatings.

## 5. Conclusions

The stereometric characteristics of the pores within EB-PVD TBCs, determined via USAXS-measurement and subsequent modeling, correspond to appropriate statistically-representative values. These data were employed to model the thermal

conductivity by a non-interacting scheme resulting in predicted values that approximate well to those measured. According to the obtained thermal conductivities representing the different pore-group domains, the deepest section of the gaps between feather arms, together with the intra-columnar pores, are the principal features affecting the thermal conductivity of EB-PVD TBCs. The lowest thermal conductivity value of the “feathery” microstructure in the as-coated condition indicates the best pore configuration, i.e. deepest gaps between the feather arms, and highest volume and density with finest dimensions of the intra-columnar pores.

### Acknowledgments

The authors acknowledge the conscientious assistance of C. Kröder, J. Brien, and H. Mangers in the production of the coatings and the fruitful discussions with Dr. U. Schulz of DLR. We also would like to express our gratitude to P.R. Jemian for the assistance during the USAXS measurements. Use of the Advanced Photon Source was supported by the U. S. Department of Energy, Office of Science, Office of Basic Energy Sciences, under Contract No. W-31-109-ENG-38.

### References

- [1] J.R. Nicholls, M.J. Deakin, D.S. Rickerby, *Wear* 233–235 (1999) 352.
- [2] C.G. Levi, *Current Opinion in Solid State and Materials Science* 8 (2004) 77.
- [3] U. Schulz, C. Leyens, K. Fritscher, M. Peters, B. Saruhan-Brings, O. Lavigne, J.-M. Dorvaux, M. Poulain, R. Mévrel, M. Caliez, *Aerospace Science and Technology* 7 (2003) 73.
- [4] U. Schulz, S.G. Terry, C.G. Levi, *Materials Science and Engineering, A, Structural Materials: Properties, Microstructure and Processing* 360 (2003) 319.
- [5] K.W. Schlichting, N.P. Padture, P.G. Klemens, *Journal of Materials Science* 36 (2001) 3003.
- [6] B. Nait-Ali, K. Haberko, H. Vesteghem, J. Absi, D.S. Smith, *Journal of the European Ceramic Society* 26 (2006) 3567.
- [7] D.Y. Tzou, *International Journal of Heat and Mass Transfer* 38 (1995) 23.
- [8] W.D. Kingery, H.K. Bowen, D.R. Uhlmann, *Introduction to Ceramics*, John Wiley and Sons, New York, 1976.
- [9] T.J. Lu, C.G. Levi, H.N.G. Wadley, A.G. Evans, *Journal of the American Ceramic Society* 84 (2001) 2937.
- [10] D.D. Hass, A.J. Slifka, H.N.G. Wadley, *Acta Materialia* 49 (2001) 973.
- [11] A. Kulkarni, A. Goland, H. Herman, A.J. Allen, T. Dobbins, F. DeCarlo, J. Ilavsky, G.G. Long, S. Fang, P. Lawton, *Materials Science and Engineering, A* 426 (2006) 43.
- [12] T.A. Dobbins, A.J. Allen, J. Ilavsky, G.G. Long, A. Kulkarni, H. Herman, P.R. Jemian, 27th International Cocoa Beach Conference on Advanced Ceramics and Composites: A, The American Ceramic Society, Cocoa Beach, Florida, 2003, p. 517.
- [13] J.C. Maxwell, *A Treatise on Electricity and Magnetism*, Dover, New York, 1954.
- [14] B. Shafiro, M. Kachanov, *Journal of Applied Physics* 87 (2000) 8561.
- [15] J. Ilavsky, A.J. Allen, G.G. Long, P.R. Jemian, *Review of Scientific Instruments* 73 (2002) 1.
- [16] J. Ilavsky, A.J. Allen, A. Kulkarni, H. Herman, *International Thermal Spray Conference*, Basel, Switzerland, 2005.
- [17] T. Krell, *Institut für Metallkunde und Metallphysik*, Rheinisch-Westfälische Technische Hochschule, Aachen, 2000, p. 179.
- [18] Y.S. Touloukian, E.H. Buyco, *Specific Heat- Nonmetallic Solids*, IFI/Plenum, New York–Washington, 1970.
- [19] S.G. Terry, *Materials Department*, University of California, 2001, p. 197.
- [20] A.F. Renteria, B. Saruhan, *Journal of the European Ceramic Society* 26 (2006) 2249.